JOURNAL OF SOLID STATE CHEMISTRY 116, 409–421 (1995)

Crystal Structure and Conductivity of the New Superionic Conductors $Ag_4Zr_3S_8$ and $Ag_{3.8}Sn_3S_8$

Olivier Amiel,[1] Daniel C. Frankel, and Hiroaki Wada

National Institute for Research in Inorganic Materials, 1-1 Namiki, Tsukuba-shi, Ibaraki 305, Japan

Received September 9, 1994; accepted September 12, 1994

The new superionic conductors $Ag_4Zr_3S_8$ and $Ag_{3.8}Sn_3S_8$ crystallize both in cubic space groups with lattice parameters a = 10.9427(3) Å ($P4_332$, Z = 4, and ρ = 4.87 g cm^{-3}) and a = 10.8013(4) Å ($P4_132$, Z = 4, and ρ = 5.39 g cm^{-3}), respectively. These compounds have similar sulfur packing consisting of sulfur octahedra sharing common edges. In both cases the M cations, either Zr or Sn, are located inside the sulfur octahedra (12*d* sites). The main crystallographic difference between the two structures is the silver packing. In $Ag_4Zr_3S_8$ the silver ions are located in three different tetrahedral sites, two of them being partially occupied. For $Ag_{3.8}Sn_3S_8$ the silver ions are exclusively situated in statistically occupied octahedral sites (12*d* and 4*b* sites) giving a rock-salt-type lattice. From the properties point of view, they are both mixed conductors exhibiting a relatively high ionic conductivity. The ionic σ_{Ag^+} and total conductivities were measured from room temperature to 205°C.

INTRODUCTION

In a previous paper we described the crystal structure and the conduction properties of $Ag_4Hf_3S_8$ (1). This compound crystallizes in the cubic system (space group $P4_332$) with a lattice constant a = 10.9051(2) Å (Z = 4 and ρ = 6.27 g cm^{-3}). The sulfur atoms produce octahedra, each one connected three-dimensionally with 12 other octahedra through a sharing of edges. The Hf atoms are located inside the sulfur octahedra and the Ag atoms distributed over three different sites, two of them being only partially occupied. As a consequence of this low occupancy rate (1/6), this compound exhibits a relatively high ionic conductivity.

Continuing our general survey of ternary systems including M cations belonging to the IVB transition elements, we have studied the Ag–Zr–S system and prepared the new superionic conductor $Ag_4Zr_3S_8$. At the same time, we found in the literature the existence of a similar compound, $Ag_4Sn_3S_8$, first prepared by Moh (2), then by Suguki *et al.* (3). As none of these researchers succeeded in determining the structure of $Ag_4Sn_3S_8$, it appeared challenging to determine it with the aid of the $Ag_4Hf_3S_8$ and $Ag_4Zr_3S_8$ crystallographic data.

This paper deals with the preparation, crystallographic study, and conduction properties of the new superionic conductors $Ag_xM_3S_8$ (M = Zr, Sn). The structural differences induced by the type of M cation used, either IVB ($Ag_4Zr_3S_8$) or IVA ($Ag_{3.8}Sn_3S_8$), are also discussed. A correlation between the discrepancies in ionic conductivity of these two compounds and their structural features is also proposed.

EXPERIMENTAL

Synthesis

The $Ag_4Zr_3S_8$ compound has been obtained from a stoichiometric mixture of Ag_2S (99.9%, Rare Metallic), Zr (99%, Rare Metallic), and S (99.9999%, Rare Metallic). The starting materials were mixed under a nitrogen atmosphere inside a dry box, in order to avoid oxidation, and ground in an agate mortar. This mixture was pressed into pellets, introduced into a silica tube, and sealed at a pressure of less than 10^{-3} Torr. The homogeneous $Ag_4Zr_3S_8$ phase was obtained after 1 week at 650°C. Resumption of the heat treatment and even increasing the temperature to 800°C (above this temperature the cubic phase is unstable) did not produce single crystals inside the silica tube. Crystal growth was achieved using a closed chemical transport system with bromine as the transport agent. The experimental conditions for the chemical transport were as follows: the silica tube had a length of 21 cm and an inner diameter of 12 mm; the transport agent was bromine (3.2 10^{-6} mole cm^{-3}); the high temperature side was 800°C and the low temperature side was 650°C.

The starting material for the chemical transport reaction was an $Ag_4Zr_3S_8$ powder (500 mg) obtained after 10 days at 800°C. The transported crystals had a tablet-like shape and were deposited on the silica tube's low temperature side.

[1] To whom correspondence should be addressed.

0022-4596/95 $6.00

The $Ag_{3.8}Sn_3S_8$ was prepared from a stoichiometric mixture of Ag_2S (99.9%, Rare Metallic), Sn (99.99%, Rare Metallic), and S (99.9999%, Rare Metallic), in a manner similar to that described above. In the case of $Ag_{3.8}Sn_3S_8$, the tube was placed in a furnace and held at 600°C for 1 week. After this thermal treatment, the mixture was ground and heated again at 600°C for 1 week. The homogeneous phase was only obtained after the second heating stage. First attempts to prepare single crystals by resuming the heat treatment for 1 month at 600°C were not successful because Ag_2SnS_3 single crystals, which are more stable at this temperature, appeared on the surface of the pellet together with SnS_2 single crystals. Different starting materials and experimental conditions (such as higher pressure, different temperatures of preparation, and varying reaction times) did not lead to better results. Finally, $Ag_{3.8}Sn_3S_8$ single crystals grew from a starting mixture with an atomic ratio Ag : Sn : S equal to 2 : 3 : 7. As no defined compound exists between $Ag_{3.8}Sn_3S_8$ and SnS_2 (on the Ag_2S–SnS_2 line in the phase diagram), the product of composition 2 : 3 : 7 gave, after 2 weeks at 600°C, a mixture of $Ag_{3.8}Sn_3S_8$ and SnS_2 single crystals. The SnS_2 single crystals are easily recognizable as orange hexagonal platelets.

Analyses

X-ray powder diffraction intensity data were collected with a step-scan procedure using the graphite-monochromated Cu$K\alpha$ radiation of a Rigaku diffractometer (Geigerflex, RAD-2B system). In order to examine the crystal symmetry, single crystals were characterized using a Buerger precession camera from Rigaku instruments (Model 4012 K 2). The crystallographic studies were performed on an Enraf–Nonius CAD-4 diffractometer. The unit cell parameters were obtained by a least-squares analysis of the setting angles of 21 and 22 reflections automatically centered in the range of $27° \leq 2\theta(\text{Mo}K\alpha_1) \leq 32°$ for $Ag_{3.8}Sn_3S_8$ and $Ag_4Zr_3S_8$, respectively. In both cases, intensity data were collected by the $(\omega - \theta)$ scan technique. A coefficient accounting for primary and secondary isotropic extinction was refined and applied to the calculated structure factors. Absorption by integration from crystal shape in the case of $Ag_4Zr_3S_8$ and empirical absorption for $Ag_4Sn_3S_8$, as well as Lorentz–polarization corrections, were also applied to the data. Four standard reflections measured every 240 min throughout the data collection decayed by 0.5% and 0.9% on average by the end of the data collection for $Ag_4Zr_3S_8$ and $Ag_{3.8}Sn_3S_8$, respectively. No correction was applied for this decay. Some additional conditions for data collection are summarized in Table 1.

Chemical composition of the single crystals was determined by means of a Jeol JXA-8600MX electron microprobe, using metallic silver, ZrO_2, SnO_2, and FeS as standards for Ag, Zr, Sn, and S, respectively. In order to optimize the results, the same single crystal used for structure determination was then examined by electron probe microanalysis (EPMA). Density measurements were carried out by the immersion method described by Barker, using CCl_4 as solvent (4).

Both the ionic conductivity of silver and the total conductivity of $Ag_4Zr_3S_8$ and $Ag_{3.8}Sn_3S_8$ were measured by a dc method using a Solartron 1286 electrical interface. The measurements were made on polycrystalline samples pressed (applied pressure of 7 ton) into pellets (diameter of 7 mm). The experimental cell was introduced into a glass tube under argon atmosphere to avoid oxidation of the sample during experiments at higher temperature. Experiments were performed using a constant current (less than 10^{-3} A) and measuring the resulting voltage drop across the sample. Preliminary experiments confirmed that interfacial polarization of the interfaces was negligible under these experimental conditions.

RESULTS AND DISCUSSION

Structure Determination

Before the four-circle X-ray experiments, the X-ray powder diffraction pattern of $Ag_4Zr_3S_8$ was first refined in the cubic system, giving a preliminary lattice parameter $a = 10.9371(5)$ Å and cell volume $V = 1308.3(1)$ Å^3. Crystal symmetry and suitability for intensity data collection were then checked by means of a Buerger precession camera. The photographs indicated that $Ag_4Zr_3S_8$ crystallizes in $P4_332$ or $P4_132$ space group, both of which are characterized by the same systematic reflection condition (0 0 l; $l = 4n$). On the basis of our previous study on $Ag_4Hf_3S_8$ (1), the structure was solved in $P4_332$ with the SDP program system and refined on F^2 by a full-matrix least-squares method (5). Due to the similarities between the Hf- and Zr-compounds, the atomic positions of $Ag_4Hf_3S_8$ were used as a starting model for the refinement of $Ag_4Zr_3S_8$, replacing Hf with Zr. The conventional $R(F)$ factor for reflections with $I_0 > 1.5\,\sigma I_0$ converged to 4.71%. Refinement of the silver site occupancies resulted in the final formula of $Ag_4Zr_3S_8$, which is in good agreement with that derived from EPMA analysis. Crystallographic experimental data are given in Table 1. The final positions, the equivalent isotropic and anisotropic thermal parameters, and the site occupancies are presented in Table 2.

A preliminary unit cell and space group for $Ag_{3.8}Sn_3S_8$ were determined by the Buerger precession camera. Like $Ag_4Zr_3S_8$, systematic absences in the photographs indicated that $Ag_{3.8}Sn_3S_8$ crystallizes in $P4_332$ or $P4_132$ space group. The crystal structure of $Ag_{3.8}Sn_3S_8$ was solved and refined using the SHELXL-93 crystallographic software package (6). The positions of the silver atoms were determined from direct methods using SHELXS-86 (7). Similar M cation and sulfur packings to those of the $Ag_4Zr_3S_8$

TABLE 1
Crystal Data and Intensity Data Collection Conditions for $Ag_4Zr_3S_8$ and $Ag_{3.8}Sn_3S_8$

Chemical formula	$Ag_4Zr_3S_8$	$Ag_{3.8}Sn_3S_8$
Formula weight (g)	961.61	1022.49
Space group	$P4_332$ (No. 212)	$P4_132$ (No. 213)
a (Å)	10.9427(3)	10.8013(4)
Volume (Å^3)	1310.29(3)	1260.18(5)
Z	4	4
Calculated density (g cm^{-3})	4.87	5.39
Measured density (g cm^{-3})	4.89	5.41
Temperature of data collection (°C)	23	22
Radiation monochromated λ(Mo$K\alpha$) (Å)	0.71073	0.71073
Crystal shape	Tablet	Tablet
Crystal color	Gray-black	Gray-black
Crystal size (mm)	0.14 × 0.12 × 0.05	0.15 × 0.12 × 0.06
Linear absorption coefficient μ (cm^{-1})	92.55	131.52
Transmission factors	0.4728–0.6334	0.2237–0.3874
Scan type	$\omega - \theta$	$\omega - \theta$
Scan speed	Variable	Variable
Scan range	(0.6 + 0.35 tan θ)	1.5 (0.6 + 0.35) tan θ
2θ (max)	70°	70°
Data collected	$\pm h$, $+k$, $+l$ ($m3m$)	$\pm h$, $+k$, $+l$ ($m3$)
No. of reflections measured	1252	2258
No. of reflections measured (with $I_0 > 0$)	1023	1963
No. of unique reflections	983	896
No. of refined reflections with $I_0 > 1.5\,\sigma I_0$	599	743
No. of variables	40	34
S(Goodness of fit on F^2)	1.337	1.777
R_{int}	0.0260	0.0424
R (F)	0.0471	0.0318
wR (F)	0.0523	0.0329
$\rho_{min} - \rho_{max}$ (e/Å^3)	−3.375 + 2.420	−0.954 + 3.539

TABLE 2
Atomic Coordinates, Site Types and Occupancies, Equivalent Isotropic and Anisotropic Thermal Factors for $Ag_4Zr_3S_8$

	Atom					
	Zr	Ag_1	Ag_2	Ag_3	S_1	S_2
Wyckoff notation	12d	8c	24e	24e	24e	8c
x	0.625	0.00511(6)	0.3139(8)	0.2133(6)	0.3909(2)	0.8699(1)
y	0.11672(6)	0.00511(6)	0.1787(8)	−0.0170(5)	+0.0954(2)	0.8699(1)
z	0.13328(6)	0.00511(6)	0.9622(8)	0.3289(7)	0.1436(2)	0.8699(1)
Site occupancy	1	1	0.1182	0.2187	1	1
U(1, 1)	18.5(3)	32.9(2)	152(6)	95(3)	13.0(7)	14.0(4)
U(2, 2)	15.0(2)	32.9(2)	145(8)	59(3)	14.8(6)	14.0(4)
U(3, 3)	15.0(2)	32.9(2)	118(4)	137(7)	46(1)	14.0(4)
U(1, 2)	−1.2(3)	−2.8(3)	48(5)	62(2)	1.4(6)	−0.5(6)
U(1, 3)	−1.2(3)	−2.8(3)	−92(3)	59(3)	2.3(8)	−0.5(6)
U(2, 3)	−1.2(3)	−2.8(3)	26(4)	25(3)	−6.3(7)	−0.5(6)
U (eq)[a]	16.2(1)	32.85(6)	138(3)	97(2)	24.5(4)	14.0(1)

[a] $U_{(eq)} = [\frac{1}{3} \sum_i \sum_j U_{ij} a_i^* a_j^* a_i a_j]^{1/2} = [1/6\pi^2 \sum_i \sum_j B_{ij} a_i a_j]^{1/2}$.

TABLE 3
Atomic Coordinates, Site Types and Occupancies, Equivalent Isotropic and Anisotropic Thermal Factors for $Ag_{3.8}Sn_3S_8$

	Atom					
	Sn	Ag_1	Ag_2	Ag_3	S_1	S_2
Wyckoff notation	12*d*	4*b*	12*d*	12*d*	24*e*	8*c*
x	0.6143(1)	0.125	0.3515(6)	0.3551(4)	0.1376(1)	0.1276(1)
y	0.8643(1)	0.375	0.6015(6)	0.6051(4)	0.8898(1)	0.1276(1)
z	0.625	0.625	0.625	0.625	0.9012(2)	0.1276(1)
Site occupancy	1	0.9940	0.4744	0.4744	1	1
U(1, 1)	11(1)	42(1)	37(3)	23(2)	20(1)	11(1)
U(2, 2)	11(1)	42(1)	37(3)	23(2)	11(1)	11(1)
U(3, 3)	11(1)	42(1)	38(4)	13(2)	10(1)	11(1)
U(1, 2)	2(1)	13(1)	6(3)	−8(2)	0(1)	−1(1)
U(1, 3)	0(1)	−13(1)	−11(2)	−10(1)	0(1)	−1(1)
U(2, 3)	0(1)	13(1)	11(2)	10(1)	−1(1)	−1(1)
U (eq)[a]	11(1)	42(1)	37(2)	20(1)	14(1)	11(1)

[a] $U_{(eq)} = [\frac{1}{3}\sum_i\sum_j U_{ij}a_i^*a_j^*a_ia_j]^{1/2} = [1/6\pi^2\sum_i\sum_j B_{ij}a_ia_j]^{1/2}$.

structure were used as preliminary positions for refinement. After refinement of the model with isotropic thermal parameters on each site, an empirical absorption correction using the program DIFABS (8) was applied. In contrast to the Hf and Zr structures, the $Ag_{3.8}Sn_3S_8$ structure was refined in the space group $P4_132$ which gave slightly lower *R* values than the refinement in $P4_332$. Final least-squares refinement on F^2, with anisotropic thermal parameters for all the atoms, resulted in the final residuals $R = 3.18\%$ and $R_w = 3.29\%$. The exact silver content was determined in the same way as that of $Ag_4Zr_3S_8$, by refinement of the silver site occupancies. The final formula converged at $Ag_{3.8}Sn_3S_8$, in good agreement with that derived from EPMA analysis ($Ag_{3.7}Sn_3S_8$). The final cell constant and additional relevant crystal data are given in Table 1. The refined atomic positional parameters, equivalent isotropic and anisotropic thermal parameters, and the site occupancies are given in Table 3.

The results of the single crystal X-ray structure determination were used to calculate the X-ray powder diffraction patterns using the program RIETAN (9). Tables 4 and 5 show a comparison of the calculated and observed X-ray powder intensities for $Ag_4Zr_3S_8$ and $Ag_{3.8}Sn_3S_8$, respectively.

Structure Description

$Ag_4Zr_3S_8$ structure. The structures of $Ag_4Zr_3S_8$ and $Ag_4Hf_3S_8$ are isomorphous, which is not surprising as both Zr and Hf belong to the same IVB period. The 32 sulfur atoms distributed over two different fully occupied positions, 24*e* and 8*c*, produce 32 octahedra in the unit cell (Fig. 1). Each octahedron is connected three-dimensionally with 12 other octahedra through common edges. As in the hafnium structure, the zirconium atoms are distributed over the 12*d* positions, and are located inside sulfur octahedra. The ZrS_6 octahedra form layers parallel to the *ab* plane (Fig. 2). Within the same ZrS_6 layer, octahedra are linked together by edges and the sequence –3 octahedra–vacancy–3 octahedra– is observed. From one ZrS_6 layer to the next (along the *c*-axis), octahedra share edges and the three-dimensional packing is alternatively along the [1 1 0] and the [$\bar{1}$ 1 0] directions (Fig. 2). As the Zr–S and the Hf–S bonds have a similar ionicity, the difference in sizes of the octahedra must be interpreted in terms of ionic radius. The size of Zr^{4+} is slightly larger than that of Hf^{4+} (10). Therefore, the bond lengths within a Zr^{4+}-containing octahedron are longer than those within an Hf^{4+}-containing octahedron (Table 6).

Ag1 silver atoms are distributed over 8*c* positions and located in nearly regular sulfur tetrahedra (Fig. 1). In each AgS_4 elementary tetrahedron, the Ag1 silver atom is surrounded by three S1 sulfurs and one S2 sulfur. The distances between Ag1 and S1 are all equal to 2.541(2) Å whereas that between Ag1 and S2 is a little longer and equal to 2.562(1) Å, as shown by the selected bond lengths and angles presented in Table 7. Silver atoms Ag2 and Ag3 are distributed over two statistically occupied 24*e* general positions. It is noteworthy that the displacement

TABLE 4
Indexed X-Ray Powder Pattern for $Ag_4Zr_3S_8$

h k l	d_0 (Å)	d_c (Å)	I/I_0	I/I_c
1 1 0	7.756	7.733	2	2
1 1 1	6.312	6.315	4	3
2 1 0	4.874	4.891	<1	<1
2 1 1	4.449	4.465	2	1
2 2 0	3.870	3.867	13	13
2 2 1	3.645	3.646	3	4
3 1 0	3.469	3.459	5	3
3 1 1	3.300	3.298	100	100
2 2 2	3.162	3.157	4	2
3 2 1	2.927	2.923	3	3
4 0 0	2.736	2.734	11	11
4 1 0	2.653	2.653	2	2
3 2 2		2.653	3	3
4 1 1	2.583	2.578	4	4
3 3 0		2.578	<1	<1
4 2 0	2.446	2.446	<1	<1
4 2 1	2.387	2.387	11	11
3 3 2	2.346	2.332	<1	<1
4 2 2	2.233	2.233	17	17
4 3 0	2.187	2.187	<1	<1
5 1 0	2.146	2.145	6	5
4 3 1		2.145	6	6
3 3 3	2.106	2.105	2	2
5 1 1		2.105	16	15
4 3 2	2.031	2.031	1	1
5 2 0		2.031	7	6
5 2 1	1.999	1.997	6	5
4 4 0	1.934	1.933	41	38
5 2 2	1.900	1.904	<1	<1
4 4 1		1.904	2	2
5 3 0	1.877	1.876	3	2
4 3 3		1.876	<1	<1
5 3 1	1.850	1.849	<1	<1
4 4 2	1.823	1.823	<1	<1
6 1 0	1.800	1.798	3	2
5 3 2	1.774	1.774	1	1
6 1 1		1.774	<1	<1
6 2 0		1.729	5	4
6 2 1	1.708	1.708	<1	<1
5 4 0		1.708	<1	<1
4 4 3		1.708	<1	<1
5 4 1	1.688	1.688	2	2
5 3 3	1.668	1.668	10	11
6 2 2	1.645	1.649	1	1
6 3 0	1.631	1.630	<1	<1
5 4 2		1.630	2	2
6 3 1	1.614	1.613	<1	<1
4 4 4	1.579	1.579	3	3
6 3 2	1.563	1.562	<1	<1
7 1 0	1.547	1.547	1	1
5 4 3		1.547	2	2
5 5 0		1.547	<1	<1
5 5 1	1.539	1.532	<1	<1
7 1 1		1.532	<1	<1
6 4 0	1.519	1.517	<1	<1
6 4 1	1.503	1.502	2	2
7 2 0		1.502	<1	<1
7 2 1	1.490	1.488	<1	<1
5 5 2		1.488	1	1
6 4 2	1.462	1.462	5	5
7 2 2	1.450	1.449	<1	<1
5 4 4		1.449	<1	<1
7 3 0	1.438	1.436	1	1
7 3 1	1.424	1.424	5	5
5 5 3		1.424	7	7
6 5 0	1.401	1.400	<1	<1
7 3 2	1.390	1.389	<1	<1
6 5 1		1.389	<1	<1
8 0 0	1.368	1.367	2	2
7 4 0	1.358	1.357	<1	<1
8 1 0		1.357	<1	<1
6 5 2		1.357	<1	<1
7 4 1	1.347	1.346	<1	<1
8 1 1		1.346	<1	<1
5 5 4		1.346	<1	<1

ellipsoid of Ag3 is far from spherical, the displacement parameters being 0.095(1), 0.059(3), and 0.137(7) Å^2 for U_{11}, U_{22}, and U_{33}, respectively. Figure 3 shows the projection in the *ab* plane of the Ag2 and Ag3 silver atoms. These atoms form a "bow tie" shape made up of two triangles, each triangle consisting of six Ag2 and six Ag3 possible positions. Figure 4 shows the structure of one of the elementary triangles. For clarity, only the Ag3 positions are represented, but identical results are obtained for the Ag2 positions. The Ag3(2), Ag3(4), and Ag3(6) positions (Note: the numbers in brackets used to differentiate the Ag3 atoms are arbitrary and do not refer to the symmetry transformations listed in Table 7) form an equilateral triangle with each side corresponding to an Ag3–Ag3 distance of 2.770(9) Å. The Ag3(1), Ag3(3), and Ag3(5) positions also form an equilateral triangle with the same Ag3–Ag3 distance, but are located on a different plane. Bond lengths between Ag3 atoms, from one plane to the next, are alternately 1.05(1) and 2.156(9) Å. The small Ag–Ag distances between adjacent sites prevent simultaneous occupation. Two different coordination geometries may be used to describe the environment of an Ag3 (or Ag2) atom:

1. The Ag3 site may be regarded as a tetrahedron site made up of S1-type sulfur atoms exclusively, but in this case the bond Ag3(1)–S1(18), equal to 3.066(7) Å, is very long. Each Ag3 (or Ag2) tetrahedron is connected to an Ag1 tetrahedron by the sharing of a 4.250(3) Å long edge made up of S1(11) and S1(18) atoms.

2. The Ag3 site may be described as a triangular site in which the silver atom is located slightly above the plane defined by the Sl(11), Sl(16), and Sl(17) atoms (the distance from the plane was calculated to be 0.019(1) Å).

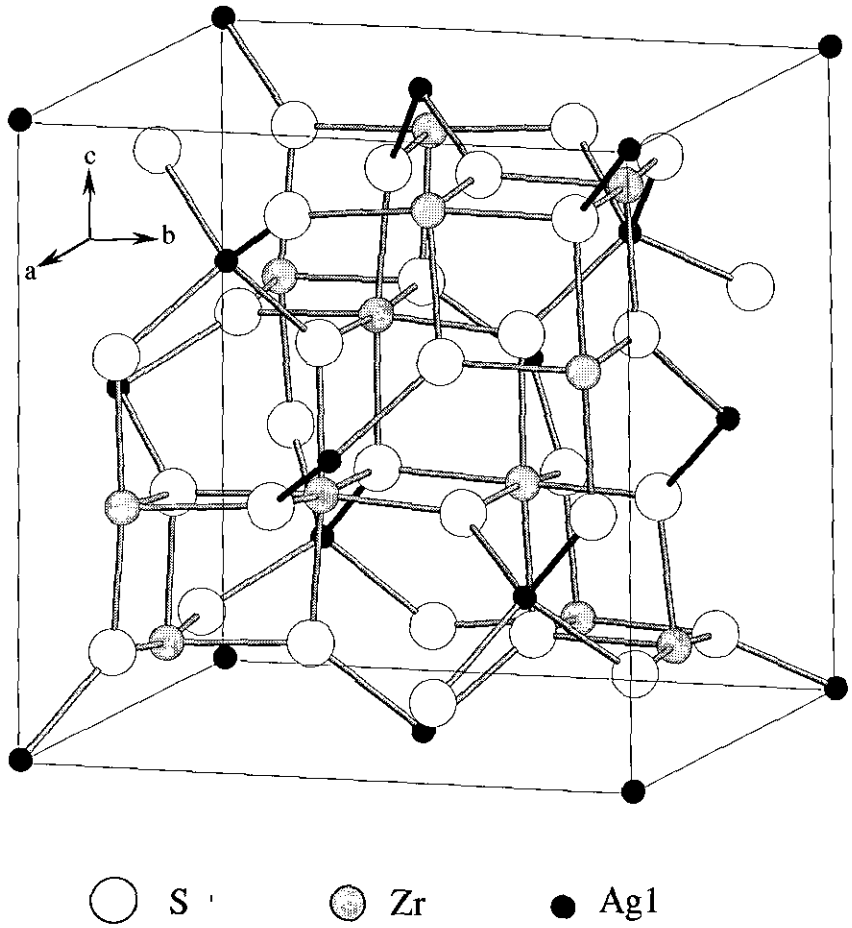

FIG. 1. Perspective view of the $Ag_4Zr_3S_8$ structure showing the packings of Zr-containing octahedra and Ag1-containing tetrahedra. For clarity, only the S, Zr, and Ag1 atoms are plotted. The unit cell is outlined.

$Ag_{3.8}Sn_3S_8$ Structure. The structures of $Ag_{3.8}Sn_3S_8$ and $Ag_4Zr_3S_8$ (or $Ag_4Hf_3S_8$) are similar in that both are characterized by the same sulfur and *M* cation packings. Figure 5 provides a perspective view of the $Ag_{3.8}Sn_3S_8$ structure. This NaCl-type structure is a three-dimensional framework of SnS_6 and AgS_6 octahedra. All the SnS_6 and AgS_6 (except Ag3) octahedra are distorted in the $Ag_{3.8}Sn_3S_8$ structure, as shown by the selected distances and angles given in Table 8. The Sn–S bond lengths vary from 2.538(2) to 2.614(1) Å (average value is 2.566 Å) and the S–Sn–S bond angles range from 86.87(5)° to 177.38(5)°. These values are comparable to those found in the literature. For example, average Sn–S bond lengths for some tin sulfide compounds in which the Sn is octahedrally coordinated range from 2.55 to 2.57 Å (11). The Ag–S bond lengths range from 2.593(2) to 2.943(7) Å and compare well with those in the literature. For example, the Ag–S bond lengths for octahedrally coordinated Ag vary from 2.45(9) to 3.20(3) Å in $AgTaS_3$ (12), and from 2.713(2) to 2.865(2) Å in $Ag_{1/2}V_{1/2}PS_3$ (13).

The Sn atoms are bonded to six S atoms at the corners of an octahedron. This type of coordination is unusual for Sn^{4+} which is more frequently encountered in tetrahedral sites (11, 14). In the same manner as for the Zr-compound described above, these Sn-containing octahedra are connected by edge-sharing and form layers along the *ab* plane. These layers are also connected along the *c*-axis by common edges. The Sn^{4+} octahedra are less distorted than those containing Zr^{4+} (Fig. 6). For the angles which would ideally be 90°, the largest deviations are the S1(3)–Sn–S2(6) angle (86.87(5)°) and the S1(7)–Zr–S2(3) angle (83.73(5)°) for $Ag_{3.8}Sn_3S_8$ and $Ag_4Zr_3S_8$, respectively. This distortion can be largely attributed to the M^{4+}–M^{4+} repulsion across the shared octahedron edge. On going from $Ag_4Zr_3S_8$ to $Ag_{3.8}Sn_3S_8$, the angular distortion is smaller, which can be explained by a decrease in the M^{4+}–M^{4+} repulsion due to an increase in the covalency of the *M*–S bond.

The most significant difference between the two structures lies in the silver packing. In $Ag_{3.8}Sn_3S_8$, the silver atoms are exclusively located in octahedral sites whereas in $Ag_4Zr_3S_8$, they are only located in tetrahedral ones. This

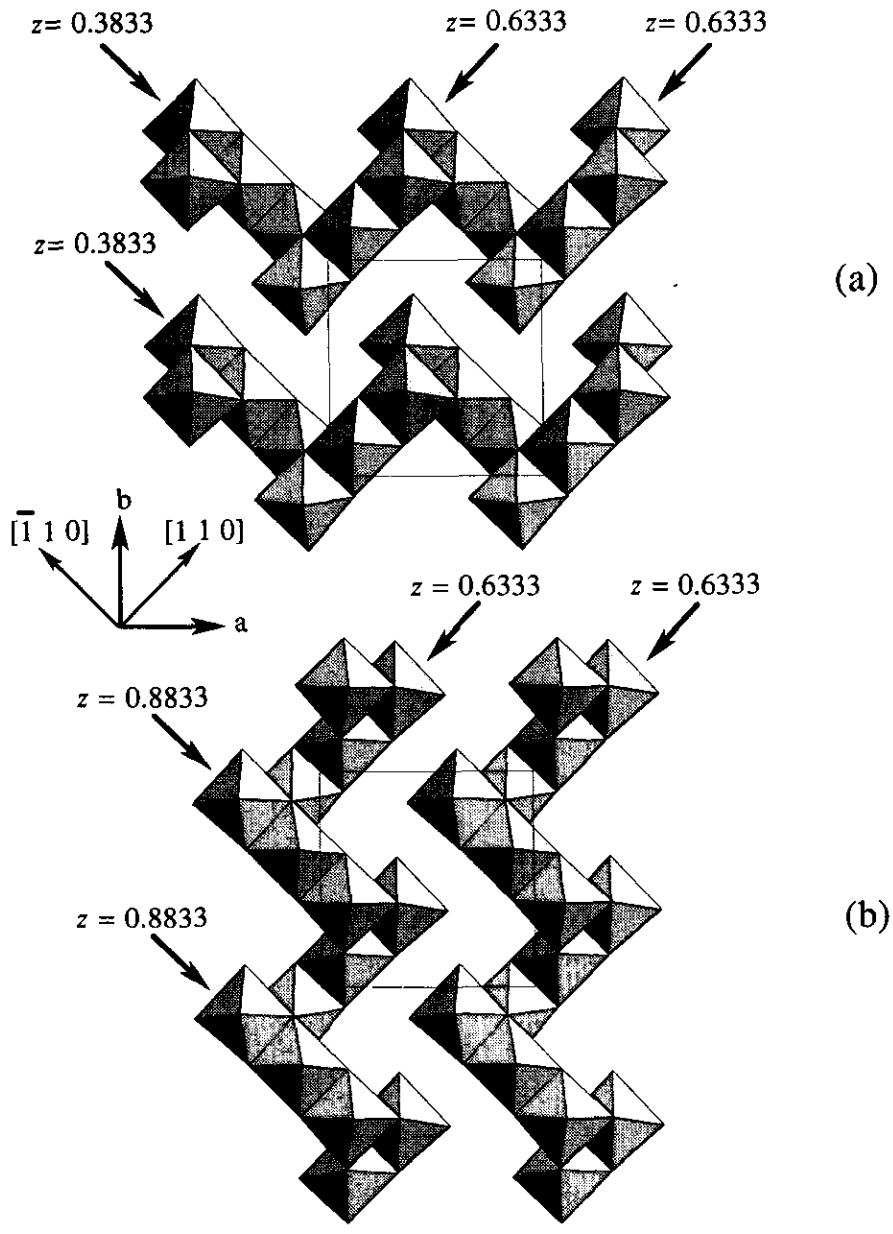

FIG. 2. Three-dimensional packing of Zr-containing octahedra. Projection in the *ab* plane of (a) the superposition of the cross sections at $z = 0.6333$ and $z = 0.3833$; (b) the superposition of the cross sections at $z = 0.6333$ and $z = 0.8833$.

octahedral coordination is unusual because in superionic conductors Ag atoms are more commonly located in sites of lower coordination such as tetrahedral or triangular environments. In the $Ag_{3.8}Sn_3S_8$ structure, the Ag atoms are distributed over three different sites. Two of them (Ag2 and Ag3) are 12*d* partially occupied positions (occupancy of 0.4744). The octahedra containing Ag2 and Ag3 atoms are linked in the same manner as those containing tin atoms. In addition to the unusual coordination about the Ag atoms, the third kind of silver atom, Ag1, is located in the special 4*b* positions for which atomic coordinates are fixed. This type of position is rare for Ag ions which are very mobile and therefore are commonly located in more general positions (like 12*d* or 24*e*) for which positional shifts are allowed. This is the reason that the thermal parameters of Ag1 are bigger than those of Ag2 and Ag3. In contrast to Ag2 and Ag3, the octahedra containing Ag1 silver atoms are regular with a single Ag1–S distance equal to 2.855(1) Å.

Silver aggregates in $Ag_4Zr_3S_8$ and in $Ag_{3.8}Sn_3S_8$. The tendency of silver ions to form aggregates is noteworthy

TABLE 5
Indexed X-Ray Powder Pattern for $Ag_{3.8}Sn_3S_8$

$h\ k\ l$	d_0 (Å)	d_c (Å)	I/I_0	I/I_c
1 1 0	7.649	7.632	9	9
1 1 1	6.241	6.231	10	9
2 1 0	4.834	4.827	8	7
2 1 1	4.414	4.406	10	10
2 2 1	3.602	3.598	6	6
3 1 0	3.417	3.413	5	4
3 1 1	3.257	3.254	7	4
2 2 2	3.119	3.116	58	55
3 2 0	2.998	2.993	5	4
3 2 1	2.888	2.884	4	2
4 0 0	2.701	2.698	100	100
4 1 0	2.618	2.618	10	10
3 3 1	2.478	2.476	1	2
4 2 1	2.358	2.355	1	1
4 3 0	2.160	2.158	4	5
5 1 0	2.119	2.117	1	1
4 3 1		2.117	1	1
3 3 3	2.080	2.077	1	1
5 1 1		2.077	3	3
4 3 2	2.006	2.004	3	2
5 2 1	1.972	1.970	7	4
4 4 0	1.910	1.908	59	61
5 2 2	1.880	1.879	1	1
4 4 1		1.879	6	6
5 3 0	1.852	1.851	1	1
5 3 1	1.826	1.824	4	3
6 1 0	1.776	1.774	<1	<1
5 3 2	1.752	1.751	3	3
6 2 1	1.686	1.686	5	5
5 4 0		1.686	2	2
4 4 3		1.686	4	4
5 3 3	1.647	1.646	<1	<1
6 2 2	1.628	1.627	27	23
6 3 0	1.606	1.609	<1	<1
5 4 2		1.609	<1	<1
4 4 4	1.559	1.558	22	18
6 3 2	1.543	1.542	2	1
7 1 0	1.527	1.526	<1	<1
5 4 3		1.526	1	1
5 5 0		1.526	<1	<1
5 5 1	1.512	1.511	2	2
7 1 1		1.511	<1	<1
6 4 2	1.442	1.442	<1	<1
7 2 2	1.427	1.423	<1	<1
5 4 4		1.423	2	2
7 3 0	1.417	1.417	<1	<1
7 3 1	1.406	1.405	1	1
5 5 3		1.405	1	1
6 5 1	1.371	1.371	1	<1
8 0 0	1.350	1.349	6	6

and seems independent of the nature of the anion. Jansen observed the same behavior for the case of silver ternary oxide (15). The d^{10} electronic structure of the silver ions appears to be the main factor toward aggregate formation as similar results were obtained with copper (d^{10})-containing ternary systems. For $Ag_4Zr_3S_8$ and $Ag_{3.8}Sn_3S_8$, the very close positions of Ag2 and Ag3 lead, from a crystallographic point of view, to nonacceptable Ag2–Ag3 distances of 0.47(1) and 0.07(2) Å, respectively. Ag–Ag distances much shorter than twice the ionic radius of silver have been commonly observed in superionic conducting chalcogenides (16–19). In fact, the occupancy of these two sites is low, therefore an Ag2 and a neighboring Ag3 position cannot be simultaneously occupied. This structural feature illustrates the mobile character of the silver ions which migrate, in a liquid-like manner, by jumping between vacant sites even at room temperature.

Conductivity Properties of $Ag_4Zr_3S_8$ and $Ag_{3.8}Sn_3S_8$

The silver ionic conductivity was measured by a dc method using the arrangement $Ag/RbAg_4I_5$/sample/$RbAg_4I_5$/Ag, in which $RbAg_4I_5$ acts as an electron blocking layer. The experimental cell has been previously described (20). For the total conductivity measurements, the set-up was simply Ag/sample/Ag.

For $Ag_4Zr_3S_8$, log σ_{Ag+} is -3.19 at 27°C and increases linearly to -2.14 at 95°C with an activation energy of 0.306 eV (Fig. 7). From this temperature to 146°C, the ionic conductivity is almost constant. This behavior may be attributed to an energy barrier between a low temperature ordered phase and a high temperature disordered phase which is more conductive. The compound then becomes more conductive reaching a value of log σ_{Ag+} equal to -1.74 at 155°C, with an activation energy of 1.458 eV. In the last part of the curve, the ionic conductivity log σ_{Ag+} increases linearly to -1.41 at 205°C, with an activation energy of 0.271 eV, similar to that observed in the first part of the curve. The total conductivity curve also displays a plateau starting at the same temperature as the ionic conductivity curve (95°C), but ending at 115°C. Comparison of the ionic and total conductivity curves shows that $Ag_4Zr_3S_8$ is a mixed conductor.

Experimental results obtained from ionic and total conductivity measurements for $Ag_{3.8}Sn_3S_8$ are plotted in Fig. 8. The value of log σ_{Ag+} is -4.14 at 25°C and increases linearly to -2.44 at 141°C, with an activation energy of

TABLE 6
M-Containing Octahedron Bond Lengths and *M* Ionic Radius for $Ag_4Zr_3S_8$ and $Ag_4Hf_3S_8$

Compound	*M*–S bond lengths	Average *M*–S bond (Å)	*M* ionic radius (Å)
$Ag_4Hf_3S_8$	2 × 2.495(2) Å 2 × 2.550(2) Å 2 × 2.577(2) Å	2.541	Hf^{4+} = 0.71
$Ag_4Zr_3S_8$	2 × 2.512(2) Å 2 × 2.575(2) Å 2 × 2.594(1) Å	2.560	Zr^{4+} = 0.72

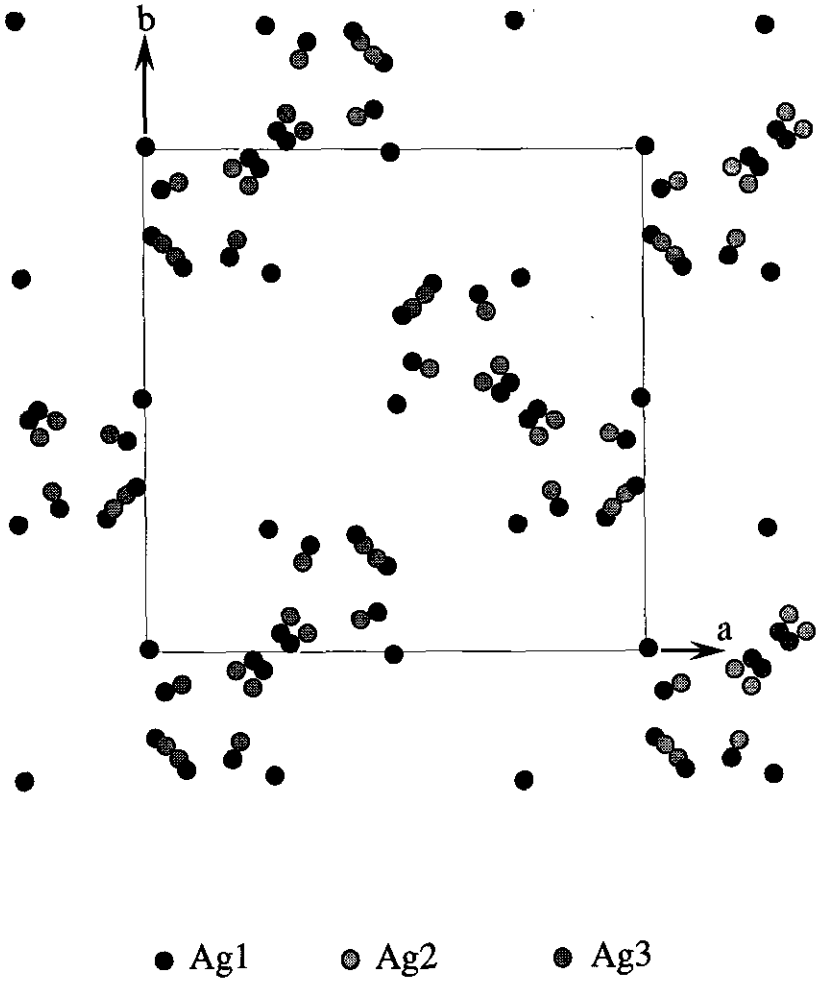

FIG. 3. Projection in the *ab* plane of the Ag1, Ag2, and Ag3 atoms.

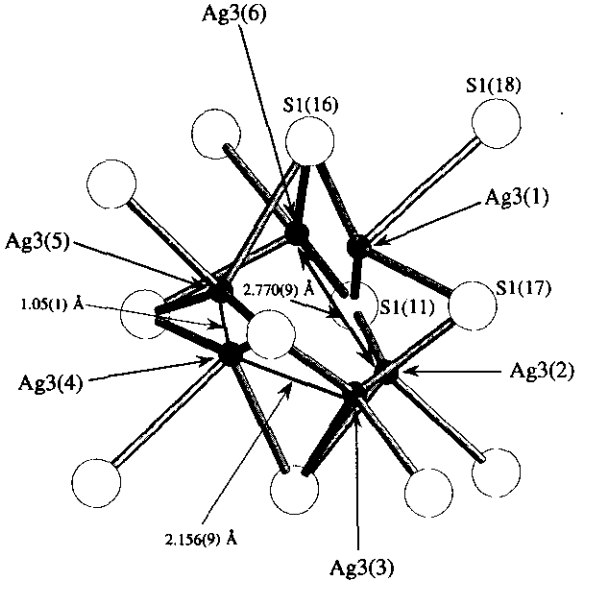

FIG. 4. Structure of an elementary triangle of Ag3 atoms.

TABLE 7
Selected Interatomic Distances and Bond Angles for $Ag_4Zr_3S_8$

Interatomic distances	(Å)	Interatomic distances	(Å)
Zr–S1(4)	2.512(2)	Ag2–S1(14)	2.722(9)
Zr–S1(6)	2.512(2)	–S1(15)	3.315(9)
Zr–S1(7)	2.575(2)	–S1(12)	2.341(9)
Zr–S1(1)	2.575(2)	–S1(13)	2.550(9)
Zr–S2(5)	2.594(1)	S1(14)–S1(15)	3.612(3)
Zr–S2(3)	2.594(1)	–S1(12)	4.628(3)
		–S1(13)	3.809(3)
Angles	(°)	S1(15)–S1(12)	4.250(3)
S1(1)–Zr–S1(6)	90.47(6)	–S1(13)	3.680(3)
S1(1)–Zr–S1(7)	169.08(6)	S1(12)–S1(13)	4.451(3)
S1(1)–Zr–S2(3)	89.00(6)		
S1(1)–Zr–S2(5)	83.73(5)	Angles	(°)
S1(1)–Zr–S1(4)	96.98(7)	S1(14)–Ag2–S1(15)	72.7(2)
S1(6)–Zr–S1(7)	96.98(7)	S1(14)–Ag2–S1(12)	132.0(4)
S1(6)–Zr–S2(3)	84.98(4)	S1(14)–Ag2–S1(13)	92.5(3)
S1(6)–Zr–S2(5)	173.98(6)	S1(12)–Ag2–S1(15)	95.9(3)
S1(6)–Zr–S1(4)	94.18(6)	S1(12)–Ag2–S1(13)	131.0(4)
S1(7)–Zr–S2(3)	83.73(5)	S1(15)–Ag2–S1(13)	76.5(2)
S1(7)–Zr–S2(5)	89.00(6)		
S1(7)–Zr–S1(4)	90.47(6)		
S2(3)–Zr–S2(5)	96.48(1)		
S2(3)–Zr–S1(4)	173.98(6)		
S2(5)–Zr–S1(4)	84.98(4)		
Interatomic distances	(Å)	Interatomic distances	(Å)
Ag1–S1(8)	2.541(2)	Ag3–S1(17)	2.860(7)
–S1(9)	2.541(2)	–S1(18)	3.066(7)
–S1(2)	2.541(2)	–S1(11)	2.283(6)
–S2(10)	2.562(1)	–S1(16)	2.504(7)
S1(8)–S1(9)	4.249(3)	S1(17)–S1(18)	4.250(3)
–S1(2)	4.249(3)	–S1(11)	4.451(3)
–S2(10)	4.051(2)	–S1(16)	4.628(3)
S1(9)–S1(2)	4.249(3)	S1(18)–S1(11)	3.680(3)
–S2(10)	4.051(2)	–S1(16)	3.612(3)
S1(2)–S2(10)	4.051(2)	S1(11)–S1(16)	3.809(3)
Angles	(°)	Angles	(°)
S1(8)–Ag1–S1(9)	113.47(6)	S1(17)–Ag3–S1(18)	76.7(2)
S1(8)–Ag1–S1(2)	113.47(6)	S1(17)–Ag3–S1(11)	119.4(3)
S1(8)–Ag1–S2(10)	105.10(5)	S1(17)–Ag3–S1(16)	90.2(2)
S1(9)–Ag1–S1(2)	113.47(6)	S1(11)–Ag3–S1(18)	104.2(2)
S1(9)–Ag1–S2(10)	105.10(5)	S1(11)–Ag3–S1(16)	150.3(3)
S1(2)–Ag1–S2(10)	105.10(5)	S1(18)–Ag3–S1(16)	80.1(2)

Note. Symmetry transformations used to generate equivalent atoms: (1) x, y, z; (2) $-y + 1/4, -x + 1/4, -z + 1/4$; (3) $y - 1/4, -x + 3/4, z - 3/4$; (4) $-z + 3/4, y + 1/4, x - 1/4$; (5) $-x + 3/2, -y + 1, z - 1/2$; (6) $z + 1/2, -x + 1/2, -y$; (7) $-x + 5/4, -z + 1/4, -y + 1/4$; (8) $-z + 1/4, -y + 1/4, -x + 1/4$; (9) $-x + 1/4, -z + 1/4, -y + 1/4$; (10) $x - 1, y - 1, z - 1$; (11) $-x + 1/4, -z + 5/4, -y + 1/4$; (12) $x, y, z + 1$; (13) $-z + 1/4, -y + 1/4, -x + 5/4$; (14) $-x + 3/4, z + 1/4, y + 3/4$; (15) $z, x, y + 1$; (16) $z + 1/4, y + 3/4, -x + 3/4$; (17) $-y + 1/4, -x + 5/4, -z + 1/4$, and (18) $x, y + 1, z$.

TABLE 8
Selected Interatomic Distances and Bond Angles for $Ag_{3.8}Sn_3S_8$

Interatomic distances	(Å)	Interatomic distances	(Å)
Sn–S1(1)	2.538(2)	Ag2–S1(8)	2.598(2)
Sn–S1(2)	2.538(2)	Ag2–S1(10)	2.599(2)
Sn–S1(3)	2.546(2)	Ag2–S1(7)	2.763(5)
Sn–S1(4)	2.546(2)	Ag2–S1(11)	2.753(5)
Sn–S2(5)	2.614(1)	Ag2–S2(12)	2.935(7)
Sn–S2(6)	2.614(1)	Ag2–S2(1)	2.943(7)
Angles	(°)	Angles	(°)
S1(1)–Sn–S1(2)	92.16(7)	S1(8)–Ag2–S1(10)	167.7(4)
S1(1)–Sn–S1(3)	90.68(5)	S1(8)–Ag2–S1(7)	102.4(1)
S1(2)–Sn–S1(3)	93.45(6)	S1(10)–Ag2–S1(7)	84.8(1)
S1(1)–Sn–S1(4)	93.45(6)	S1(8)–Ag2–S1(11)	85.0(1)
S1(2)–Sn–S1(4)	90.68(5)	S1(10)–Ag2–S1(11)	102.7(1)
S1(3)–Sn–S1(4)	174.05(8)	S1(7)–Ag2–S1(11)	106.6(3)
S1(1)–Sn–S2(5)	87.05(4)	S1(8)–Ag2–S2(12)	81.5(2)
S1(2)–Sn–S2(5)	177.38(5)	S1(10)–Ag2–S2(12)	89.4(2)
S1(3)–Sn–S2(5)	89.06(4)	S1(7)–Ag2–S2(12)	166.6(3)
S1(4)–Sn–S2(5)	86.87(5)	S1(11)–Ag2–S2(12)	86.47(5)
S1(1)–Sn–S2(6)	177.38(5)	S1(8)–Ag2–S2(1)	89.2(2)
S1(2)–Sn–S2(6)	87.05(4)	S1(10)–Ag2–S2(1)	81.3(2)
S1(3)–Sn–S2(6)	86.87(5)	S1(7)–Ag2–S2(1)	86.14(5)
S1(4)–Sn–S2(6)	89.06(4)	S1(11)–Ag2–S2(1)	166.9(3)
S2(5)–Sn–S2(6)	93.85(6)	S2(12)–Ag2–S2(1)	81.0(2)
Interatomic distances	(Å)	Interatomic distances	(Å)
Ag1–S1(13)	2.855(1)	Ag3–S1(8)	2.593(2)
Ag1–S1(14)	2.855(1)	Ag3–S1(10)	2.593(2)
Ag1–S1(7)	2.855(1)	Ag3–S1(7)	2.795(4)
Ag1–S1(15)	2.855(1)	Ag3–S1(11)	2.790(4)
Ag1–S1(9)	2.855(1)	Ag3–S2(12)	2.894(5)
Ag1–S1(11)	2.855(1)	Ag3–S2(1)	2.898(5)
Angles	(°)	Angles	(°)
S1(13)–Ag1–S1(14)	101.52(7)	S1(8)–Ag3–S1(10)	170.2(3)
S1(13)–Ag1–S1(7)	96.96(6)	S1(8)–Ag3–S1(7)	101.7(1)
S1(14)–Ag1–S1(7)	80.82(5)	S1(10)–Ag3–S1(7)	84.20(9)
S1(13)–Ag1–S1(15)	80.82(5)	S1(8)–Ag3–S1(11)	84.32(9)
S1(14)–Ag1–S1(15)	96.96(6)	S1(10)–Ag3–S1(11)	101.8(1)
S1(7)–Ag1–S1(15)	176.52(6)	S1(7)–Ag3–S1(11)	104.7(2)
S1(13)–Ag1–S1(9)	176.52(6)	S1(8)–Ag3–S2(12)	82.4(1)
S1(14)–Ag1–S1(9)	80.82(5)	S1(10)–Ag3–S2(12)	90.4(1)
S1(7)–Ag1–S1(9)	80.82(5)	S1(7)–Ag3–S2(12)	168.3(2)
S1(15)–Ag1–S1(9)	101.52(7)	S1(11)–Ag3–S2(12)	86.60(4)
S1(13)–Ag1–S1(11)	80.82(5)	S1(8)–Ag3–S2(1)	90.3(1)
S1(14)–Ag1–S1(11)	176.52(6)	S1(10)–Ag3–S2(1)	82.3(1)
S1(7)–Ag1–S1(11)	101.52(7)	S1(7)–Ag3–S2(1)	86.42(4)
S1(15)–Ag1–S1(11)	80.82(5)	S1(11)–Ag3–S2(1)	168.4(2)
S1(9)–Ag1–S1(11)	96.96(6)	S2(12)–Ag3–S2(1)	82.5(2)

Note. Symmetry transformations used to generate equivalent atoms: (1) $-y + 1/2, -z + 1, x + 1/2$; (2) $-z + 3/4, -y + 3/4, -x + 3/4$; (3) $-x - 1/4. -z + 3/4, -y + 7/4$; (4) $-z + 1/2, -x, y - 1/2$; (5) $-x - 1/2, -y, z + 1/2$; (6) $-y - 1/4, -x - 1/4, -z + 3/4$; (7) $-z + 1, x + 1/2, -y + 3/2$; (8) $y - 1/2, -z + 3/2, -x + 1$; (9) $-y + 1, z - 1/2, -x + 1/2$; (10) $-z + 5/4, y - 1/4, x + 1/4$; (11) $x + 1/4, -z + 5/4, y - 1/4$; (12) $-y + 3/4, -x + 3/4, -z + 3/4$; (13) $z - 3/4, -y + 5/4, x + 3/4$; (14) $-x, y - 1/2, -z + 3/2$; and (15) $y - 3/4, -x + 1/4, z - 1/4$.

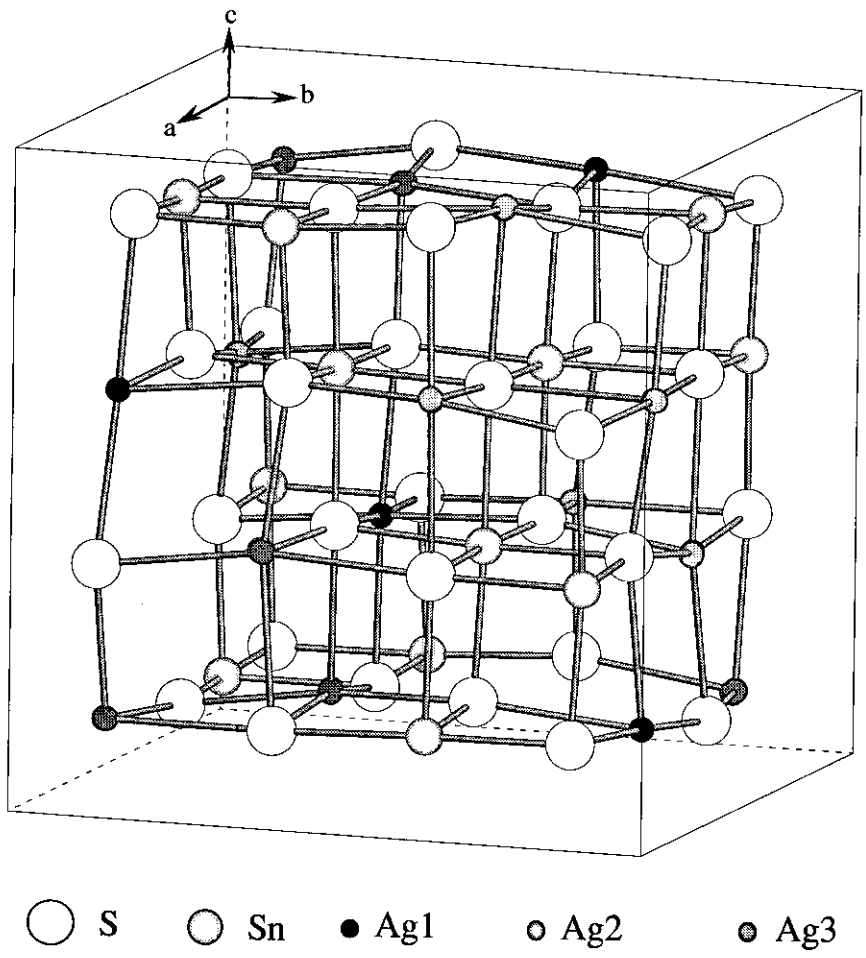

FIG. 5. Perspective view of the $Ag_{3.8}Sn_3S_8$ structure. The unit cell is outlined.

0.369 eV. For $Ag_4Zr_3S_8$, a short plateau is observed between 141 and 156°C. Surprisingly, this plateau is not followed by a steep increase in the ionic conductivity and therefore probably does not correspond to a phase transition. From the end of the plateau, the ionic conductivity log σ_{Ag+} rises to −2.00 at 205°C, with an activation energy of 0.398 eV. The similar behavior of the ionic and total conductivity curves between 25 and 105°C would suggest that electronic conductivity is almost independent of temperature in this range. The transport number of Ag^+, expressed as $\sigma_{Ag+}/(\sigma_{Ag+} + \sigma_{e-})$, was evaluated to be 0.43 between 25 and 105°C, meaning that $Ag_{3.8}Sn_3S_8$ is also a mixed conductor.

The differences in ionic conductivity for $Ag_4Zr_3S_8$ and $Ag_{3.8}Sn_3S_8$ may be correlated with the structural features of these two structures (Fig. 9). As reported in Table 9, all the Ag–Ag bond lengths are shorter for $Ag_4Zr_3S_8$, in which silver atoms are tetrahedrally coordinated. The close vicinity of Ag atom sites allows easier jumps between neighboring sites. Moreover, the occupancies of the sites available for silver atoms are much lower in the case of the Zr-compound and therefore result in a more

TABLE 9
Selected Ag–Ag Bond Lengths (Å) for $Ag_4Zr_3S_8$ and $Ag_{3.8}Sn_3S_8$

Compound	d(Ag2–Ag2)	d(Ag3–Ag3)	d(Ag1–Ag2)	d(Ag1–Ag3)
$Ag_{3.8}Sn_3S_8$	4.012(5)	3.975(3)	3.453(9)	3.515(6)
$Ag_4Zr_3S_8$	1.24(1) 1.43(1)	1.05(1) 2.156(9)	3.265(9)	3.029(6)

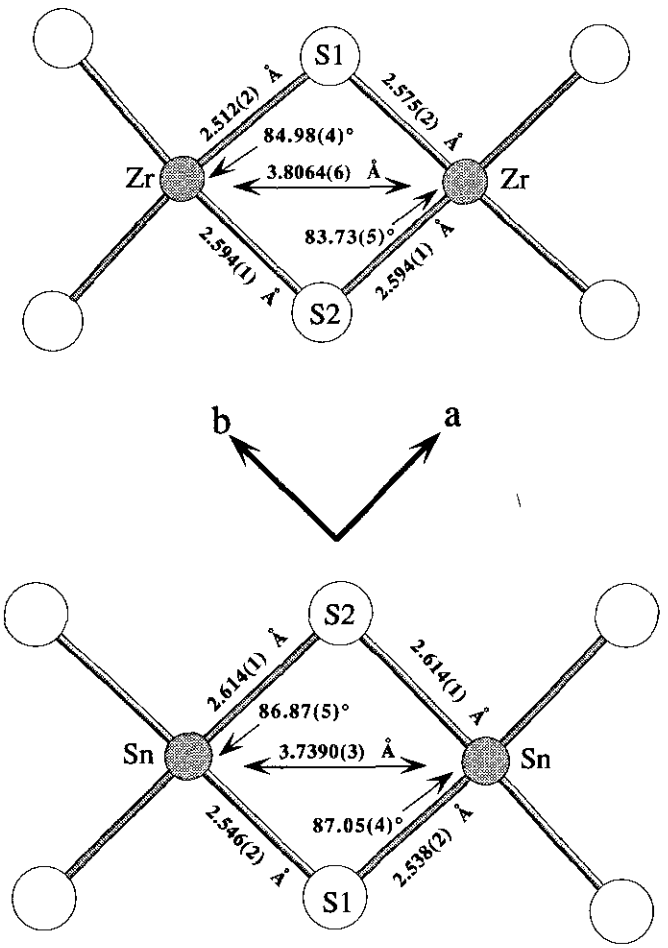

FIG. 6. Comparison of the bond lengths and angles for a Zr-containing octahedron and a Sn-containing octahedron. Projection in the *ab* plane.

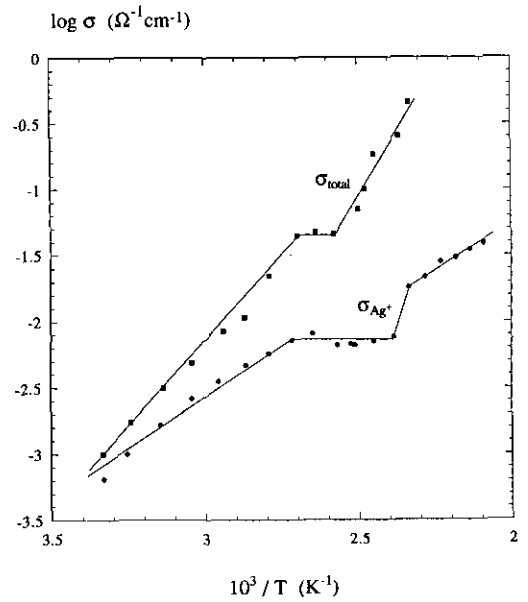

FIG. 7. Ag^+ ionic conductivity and total conductivity for $Ag_4Zr_3S_8$ versus temperature.

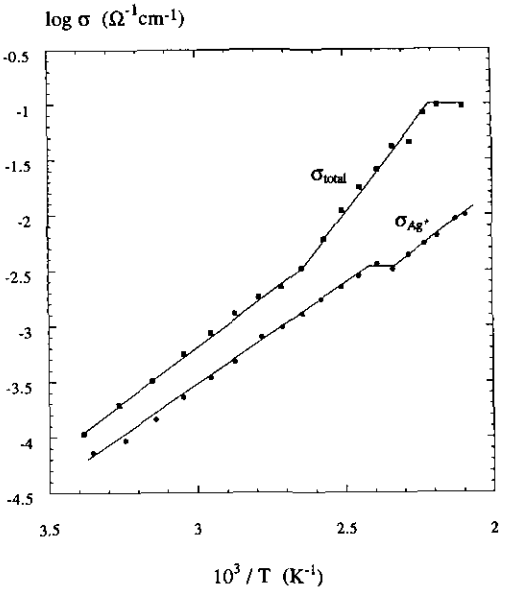

FIG. 8. Ag^+ ionic conductivity and total conductivity for $Ag_{3.8}Sn_3S_8$ versus temperature.

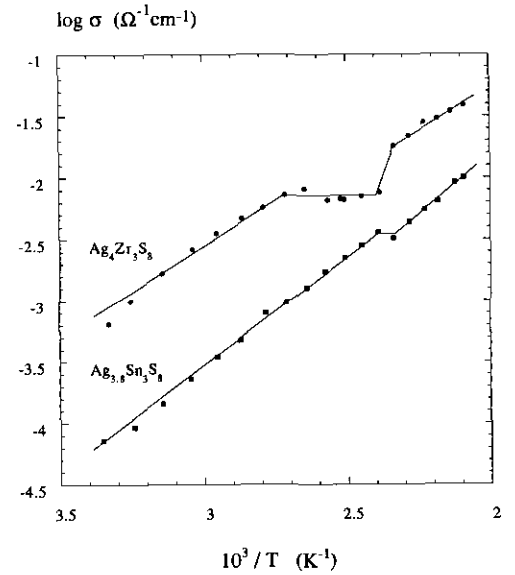

FIG. 9. Comparison of the Ag^+ ionic conductivity curves versus temperature for $Ag_4Zr_3S_8$ and $Ag_{3.8}Sn_3S_8$.

disordered arrangement of silver atoms. These two factors, namely the bond lengths and the silver site occupancies, explain why the ionic conductivity of $Ag_4Zr_3S_8$ is larger than that of $Ag_{3.8}Sn_3S_8$.

ACKNOWLEDGMENTS

The authors express sincere gratitude to M. Saeki for the use of his furnace for the $Ag_4Zr_3S_8$ single crystal synthesis, to M. Onoda for useful crystallographic discussions, and to A. Sato for collection of the single crystal X-ray data.

REFERENCES

1. O. Amiel and H. Wada, *J. Solid State Chem.* **115,** 112 (1995).
2. G. H. Moh, *N. Jb. Miner. Abh.* **131,** 33 (1977).
3. A. Sugaki, A. Kitakaze, and H. Kitazawa, *Sci. Rep. Tohoku Univ.* **16,** 199 (1985).
4. W. W. Barker, *J. Appl. Crystallogr.* **5,** 433 (1972).
5. B. A. Frenz & Associates, Inc., "SDP Structure Determination Package," 4th ed. College Station, Texas, 1985.
6. G. M. Sheldrick, in preparation.
7. G. M. Sheldrick, *Acta Crystallogr. Sect. A* **46,** 467 (1990).
8. N. Walker and D. Stuart, *Acta Crystallogr. Sect. A* **39,** 158 (1983).
9. F. Izumi, *in* "The Rietveld Method" (R. A. Young, Ed.), Chap. 13, Oxford Univ. Press, Oxford, 1993.
10. R. D. Shannon, *Acta Crystallogr. Sect A* **32,** 751 (1976).
11. J. C. Jumas, E. Philippot, and M. Maurin, *J. Solid State Chem.* **14,** 152 (1975).
12. H. Wada, M. Onoda, and H. Nozaki, *J. Solid State Chem.* **97,** 29 (1992).
13. S. Lee, P. Colombet, G. Ouvrard, and R. Brec, *Mater. Res. Bull.* **21,** 917 (1986).
14. P. Wu and J. A. Ibers, *J. Solid State Chem.* **110,** 156 (1994).
15. M. Jansen, *Angew. Chem. Int. Ed. Engl.* **26,** 1098 (1987).
16. H. Wada and M. Onoda, *J. Less-Common Met.* **175,** 209 (1991).
17. N. Rysanek, P. Laruelle, and A. Katty, *Acta Crystallogr. Sect. B* **32,** 692 (1976).
18. S. Geller, *Z. Kristallogr.* **149,** 31 (1979).
19. J. P. Deloume and R. Faure, *J. Solid State Chem.* **36,** 112 (1981).
20. H. Wada, *J. Alloys Comp.* **178,** 315 (1992).